ISSN 2278-3091
Volume 9 No.2, March -April 2020
International Journal of Advanced Trends in Computer Science and Engineering
Available Online at http://www.warse.org/IJATCSE/static/pdf/file/ijatcse74922020.pdf
https://doi.org/10.30534/ijatcse/2020/74922020

Tumor Net (T-Net) for Classification of multi Tumors in Brain MR Images

Anil Kumar B[1], P. Rajesh Kumar[2]
[1]Assistant Professor, Department of ECE, GMR Institute of Technology, India, anilkumar.b@gmrit.edu.in
[2]Professor, Department of ECE, Andhra University College of Engineering (A), India, rajeshauce@gmail.com

ABSTRACT

Identification and classification of brain tumors play an incredibly significant role in patients 'medical diagnosis and treatment plans. MR Imaging modality is most preferable for Brain images due to no ionizing radiation and superior quality of the soft tissues of the Brain. The increasing quantity of magnetic imaging brain data and substantial challenges facing by traditional methods of using small data for image classification. Deep learning (DL) has become common in image classification problems in recent years and has become powerful. A deep neural network trained from scratch is proposed in this work to classify brain tumors in two publicly available datasets. The former is Brain image datasets collected from BRATS MRI brain datasets and other one is CE-MRI. The performance of the proposed Tumor Net (T-Net) is assessed with the state of art models and T-net performance is outstanding with an accuracy of 98% for BTDS-3 dataset and 99.3% for CE-MRI dataset.

Key words: Brain tumors, Classification, CNN, Deep learning, MRI, Hyper Parameters.

1. INTRODUCTION

Brain tumors are cell growth that is abnormal and uncontrolled in the brain. The brain is surrounded by a hard core structure called the skull, which restricts the uncontrolled growth of cells in that region. The growth of abnormal cells may cause different functional problems in other organs of the body [1]. There are two groups of brain tumors that can be categorized as primary and secondary tumors. The primary tumors arise in their own brain tissues and most of them are benign and secondary tumors develop in other body organs and spread to the brain [2].

WHO (World Health Organization) specified that, 2% of overall cancers are brain tumors [3]. The identification and classification of brain tumors can be observed using various imaging techniques. MRI is therefore one of the most popular non-invasive methods. The success of MRIs stems from the fact that during scanning no ionizing radiation is used, its superior soft-tissue quality and the ability to aquire different images using different image constraints [4], [5].

Nevertheless, with the progress in brain science and brain imaging expertise, growing amounts of brain imaging data are being collected, and large quantities of samples are being collected. Modern, single-site and small-sample approaches to statistical analysis are problematic when approaching multiple center big data. The previous approaches would be unsuccessful due to large individual variations and discrepancies between centres.

With the growing number of MRI data for brain imaging, conventional methods of study are beginning to lose effectiveness. Many standard statistical techniques, such as principal component analysis (PCA), independent component analysis (ICA), and classifications dependent on feature description and feature selection strategies, such as scale invariant feature transform (SIFT) [6], 3D descriptors, support vector machine (SVM) [7] and MVPA [8] are unable to accommodate broad datasets. As traditional methods have to fed complete training data features to construct a classification model, the cost of memory becomes excessive as the total data samples proliferations to complete the computation. The deep learning methodology has an inherent advantage in tackling big data, as opposed to conventional approaches. The method of separating huge training data sets into smaller lots and using iterations to minimize feature loss by speeding up the GPU easily complies with the computational promptness requirement [9].

Academicians and industry professionals has proposed different types of deep learning models to address the image classification tasks on huge datasets such as Imagnet Challenge [10]. In this challenge different types of deep learning models are proposed like AlexNet, VGGNet, googLeNet and ResNet etc.

Over the years, the Brain tumors classi cation was conducted using various machine learning methods and imaging modalities. In some research [11] suggested a method for classifying various grades of glioma in addition to using SVMs and KNN as a hierarchical classification for high and low grades. El-Dahshan et al. [12] Developed a system to classify 80 normal and abnormal brain tumor images using Discrete Wavelet Transform (DWT) to extract features, Principal Component Analysis (PCA) to minimize features, and then ANN and KNN to classify images with 97 percent and 98 percent overall accuracy, respectively. In the year 2015.

Cheng et al. [13] suggested a method to improve brain tumor detection efficiency by growing the tumor area by

means of image dilation and subsequently splitting it into subregions. In the research work suggested by Ertosun and Rubin are used three methods to get features; Gray Level Co-occurrence Matrix (GLCM) level histogram and Bag of Words (BOW) [14], Paul et al. [15] suggested the CNN architecture consisted of 2 convolution layers with two corresponding max pooling layers and two fully connected layers with a maximum accuracy of 91.43 percent.

Afshar et al. [16] proposed a capsule network (CapsNet) that incorporates both the brain picture of MRI and the boundaries of coarse tumors to identify the brain tumor. In this analysis, 90.89% accuracy was obtained. In a different study, Anaraki et al. [17] suggested a two-state model for the classification of brain tumor images based on Genetic Algorithms and CNN with 90.9 percent accuracy was achieved in the rest case study in the classification of glioma three grades while 94.2 percent accuracy was achieved in the second case study of the glioma, meningioma and pituitary tumors classification.

2. PROPOSED T-NET

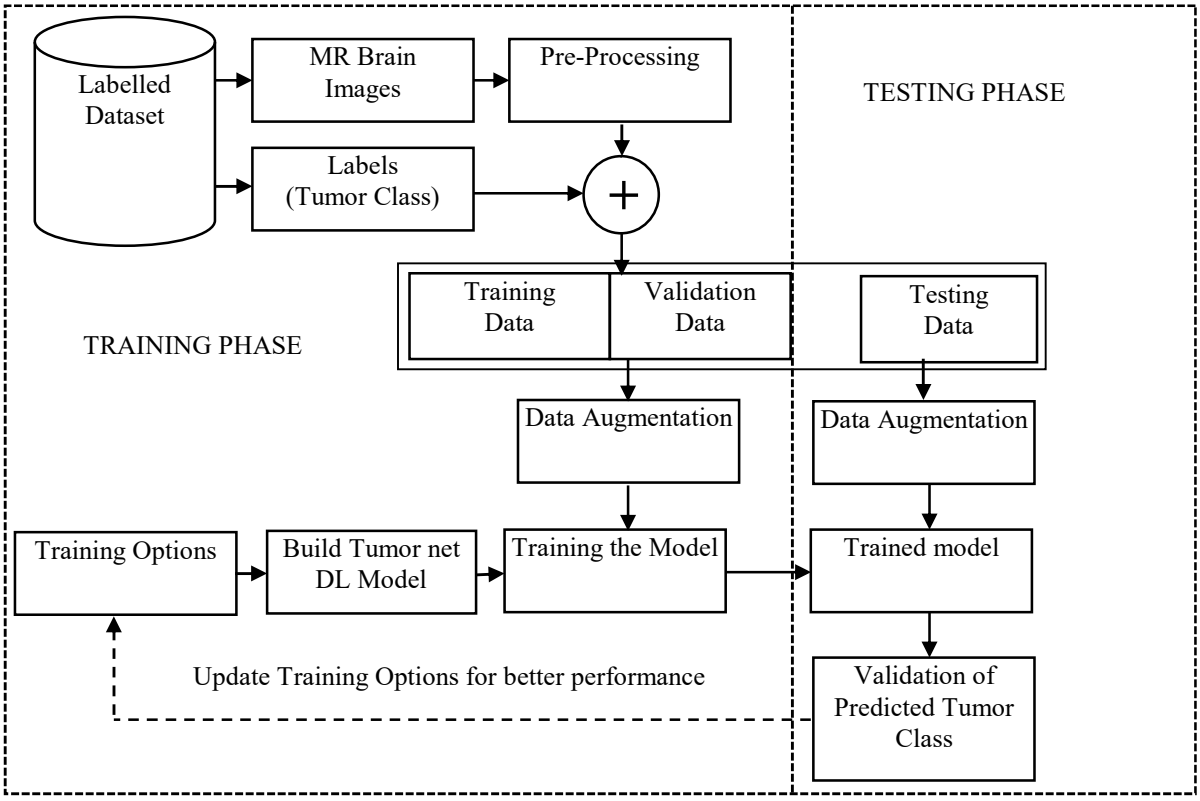

Figure 1: Training Phase and Testing Phase of proposed model

Figure 1 shows the training phase and testing phase of the T-Net model, the model loaded with extracted pre-processed BRATS dataset images and labels, then the BRATS dataset is splatted into training, Validation and testing datasets. The training and validation sets are fed to augmentation to fit into the proposed Tumor Net (T-Net) during the training phase. The structure of the proposed architecture is trained with augmented trained data and validated with validation data for every epoch. The training is performed based on the training parameters like no. of epochs, mini batch size, regularization, learning rate, etc., in the testing phase the trained model is tested on testing dataset and validated with performance metrics.

2.1 Dataset

To train a deep learning model, huge amount of data is required. Such datasets with large amount of labelled data is usually not available in medical imaging. In this work, The dataset comprises 2D slices extracted from BRATS 2015, BRATS 2017 and BRATS 2018 volumetric data to feed proposed DL model. Figure 1 shows the dataset used in this work. The BRATS 2017 & BRATS 2018 consists .nii (NIFTI) format and BRATS 2015 consists .mha (metaImage) format volumetric data [18], [19]. 2D slices of Axial, Coronal and Sagittal modes are extracted from these volumetric datasets using ITK Snap tool [20]. The complete dataset is called BTDS-3 and details are given in Table 1 and CE-MRI dataset details are in Table 2.

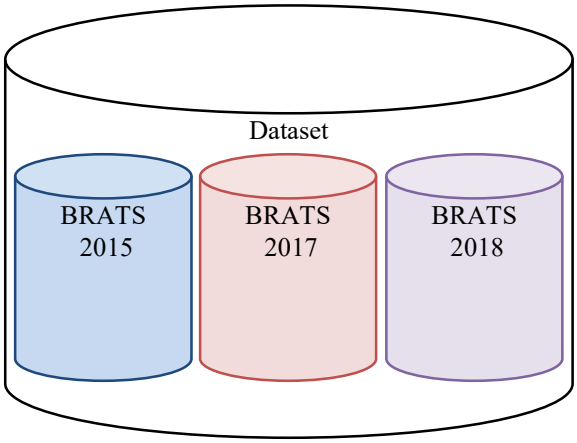

Figure 2: Collected Dataset (BTDS-3)

The BTDS-3 dataset is a combination of different BRATS datasets. Table 1 describes the complete details of dataset and the contribution of individual BRATS datasets.

Figure 3 shows the sample data from the BTDS-3 dataset. Figure 4 shows the sample data from CE-MRI.

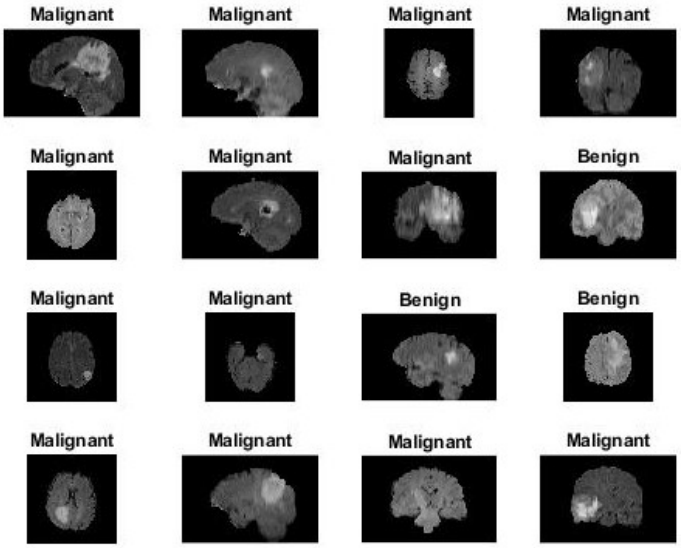

Figure 3: Sample dataset from (BTDS-3)

Table 1: Details of Collected Dataset (BTDS-3)

S.NO.	Data set	Type of tumor	Mode	No. of Images	Total No. of Images
1.	BRATS 2015	Benign	Axial	333	757
			Coronal	217	
			Sagittal	207	
		Malignant	Axial	1789	4205
			Coronal	1072	
			Sagittal	1344	
2.	BRATS 2017	Benign	Axial	340	1099
			Coronal	434	
			Sagittal	325	
		Malignant	Axial	1505	3860
			Coronal	1432	
			Sagittal	923	
3.	BRATS 2018	Benign	Axial	364	1133
			Coronal	419	
			Sagittal	350	
		Malignant	Axial	1773	4973
			Coronal	1841	
			Sagittal	1359	

2.2 Preprocessing

De-noising, data augmentation and intensity normalization are three pre-processing steps used to fit the dataset to the proposed T-Net model. Two datasets are used in this work, BTDS-3 and CE-MRI. The BTDS-3 dataset is available in PNG format and this dataset is passed through DnCNN and median filter for removing the noise. Where CE-MRI data set contain gray images, it is passed through the median filter only. This de-noising process eliminates Gaussian noise and other high frequency artifacts of images which reduces computational time.

Data Augmentation is the main aspect of transfer learning pre-processing. This involves other strategies such as resizing, tossing, situations, incorporating salt and pepper noise, streamlining, Translation, Rotation, and Perspective Transform. The BTDS-3 and CE-MRI datasets are with 240 X 240 X 3, 240 X 155 X 3, 240 X 155 X 3 and 512 X512 image sizes respectively. The BT-VGGnet image input layer size is 224 X 224 X 3. As per our proposed BT-VGGnet model only resize is required to fit the dataset into the model.

Intensity values of these datasets are not showing a static meaning. As per the observations in the datasets intensity values of MR images are varying with respect to intra and inter subjects. So Normalization is required for datasets in order to not to pull the network in ill condition. min-max normalization is used as pre-process the datasets to balance the intensity value to [0, 1] .

$$y_i = (x_i - \min(x)) / (\max(x) - \min(x)) \quad (1)$$

Where the value of normalized intensity with respect to x_i is y_i and max(x) and min(x) is the maximum and minimum intensity levels over the whole image.

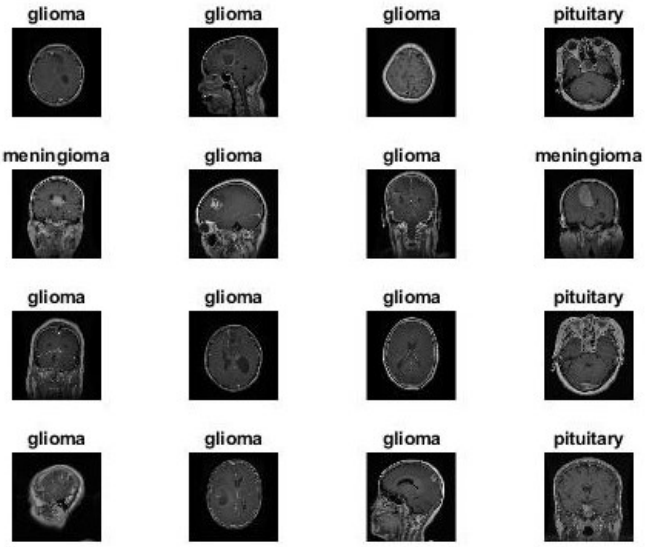

Figure 4: Sample dataset from CE-MRI

Table 2: CE-MRI Dataset Split-up

S.NO.	Data set	Type of tumor	Mode	No. of Images	Total No. of Images
1.	CE-MRI	Glioma, Meningioma and Pituitary	Axial Coronal Sagittal	3064	3064
2.	Training set	Glioma	Axial	433	1283
			Coronal	448	
			Sagittal	314	
		Meningioma	Axial	474	637
			Coronal	211	
			Sagittal	252	
		Pituitary	Axial	256	837
			Coronal	286	
			Sagittal	295	
3.	Testing set	Glioma	Axial	61	143
			Coronal	45	
			Sagittal	37	
		Meningioma	Axial	34	71
			Coronal	21	
			Sagittal	16	
		Pituitary	Axial	433	93
			Coronal	448	
			Sagittal	402	

2.3 T-Net Architecture

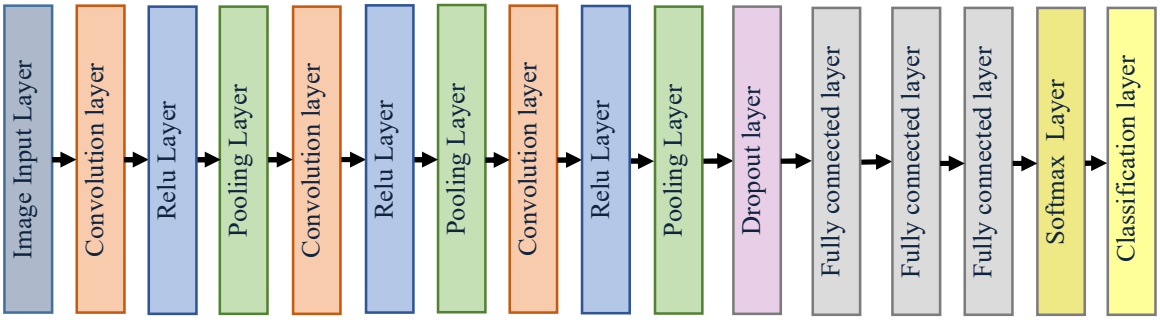

Figure 5: T-Net Architecture

Figure 5 shows the T-Net architecture and the explanation of every layer as follows. The initial layer is an image input layer which takes an image as input with specified input size and normalization is performed [21]. T-Net consists three convolution layers, with a K number of filters with filter size M X N and computes the dot product of filter and input throughout the input image. The filters move along the input image horizontally and The Stride (S) is called vertically. Padding (P) of the original images can occur before the filters are slid to keep the information to the edges. The lower level layers will take low features like lines and edges, and higher level layers will take high level features [22]. The dropout regularization is used to avoid over fitting of the network. Dropout layer is followed by fully connected, softmax and classification layers.

Table 3: Layer wise description of T-Net

Layer No.	Layer Name	Layer Type	Specifications
1	imageinput	Image Input	129x129x1
2	conv_1	Convolution	32 3x3x1
3	relu_1	ReLU	ReLU
4	maxpool_1	Max Pooling	3x3 max pooling
5	conv_2	Convolution	32 3x3x1
6	relu_2	ReLU	ReLU
7	maxpool_2	Max Pooling	3x3 max pooling
8	conv_3	Convolution	64 3x3x32
9	relu_3	ReLU	ReLU
10	maxpool_3	Max Pooling	2x2 max pooling
11	dropout	Dropout	15% dropout
12	fc_1	Fully Connected	588 fully connected layer
13	fc_2	Fully Connected	588 fully connected layer
14	fc_3	Fully Connected	2/3 fully connected layer
15	softmax	Softmax	softmax
16	classoutput	Classification Output	crossentropyex

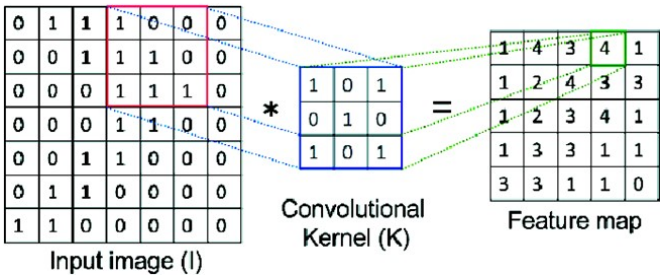

Figure 6: Convolution Layer

Figure 6 shows an example of a convolution layer with kernel and output feature map. A kernel of size 3 X 3 is applied on 7 X 7 input image and got 5 X 5 feature map. The output feature map size depends on the following equation.

$$\frac{W+2P-f}{S}+1 \text{ X } \frac{H+2P-f}{S}+1 \qquad (2)$$

Where W and H are width and height of the input image, 'p' is pooling, 'f 'is kernel size and 's' is stride value.

Following each convolution layer is a non-saturated activation function called ReLU, which is primarily used to significantly reduce the training period compared to other activation functions [23].

The following equation describes the model, ReLU as a function of x where the output is equal to the output if x is positive and 0 for other values [24]. The graphical representation of ReLU function is shown in Figure.7.

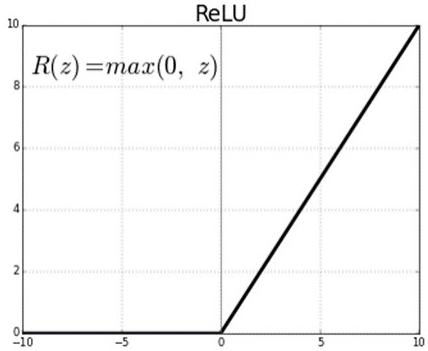

Figure 7: ReLu Activation function

The max pooling is used to down sample the feature map with a small sliding rectangle of size 3 X 3 and 2 X 2 is used in this architecture. This sliding rectangle will move throughout the previous layer and takes the max value in covering rectangle space as shown in figure 8. The pooling layer used to reduce the samples and computations [25].

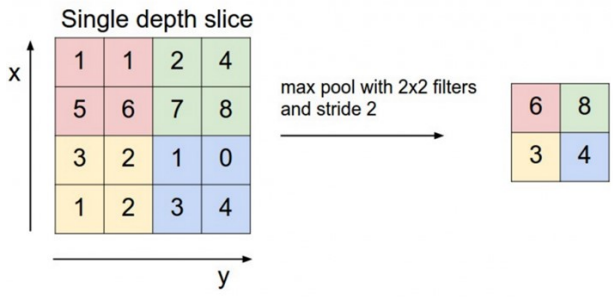

Figure 8: Max Pooling

To avoid the over fitting, dropout regularization is used with 15% dropout probability for proposed T-Net Architecture. The dropout layer drops the randomly selected activation nodes of the layers [26], which will improve the speed of the training phase. Figure 9 shows the Dropout layer.

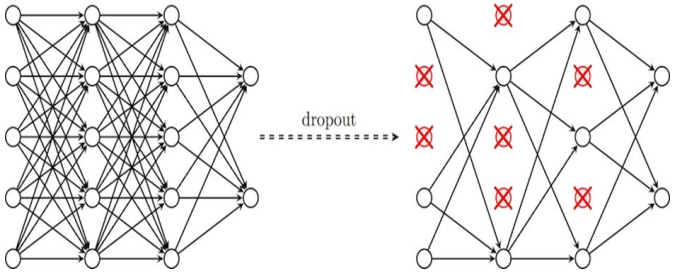

Figure 9: Dropout Layer

After the dropout layer, the fully connected layer, softmax and classification layers are connected for classification. Three fully connected layers are utilized in this deep structure. The starting two layers of size 588 each and the last one is 2 or 3 depends on the dataset classes. Every node of layer is connected to all nodes of the next layer inside the fully connected layers.

The Softmax activation layer will split the probability of predicted classes in 0 to 1. The sum of all predicted values is 1. The output of the softmax layer is calculated as follows.

$$y(z)_j = \frac{e^{z_j}}{\sum_{k=1}^{k} e^{z_k}} \tag{3}$$

The chance of any class (j) can be estimated as a function y (z) over (k) different classes and their complete summation is equal to one [27] as shown in Figure 10.

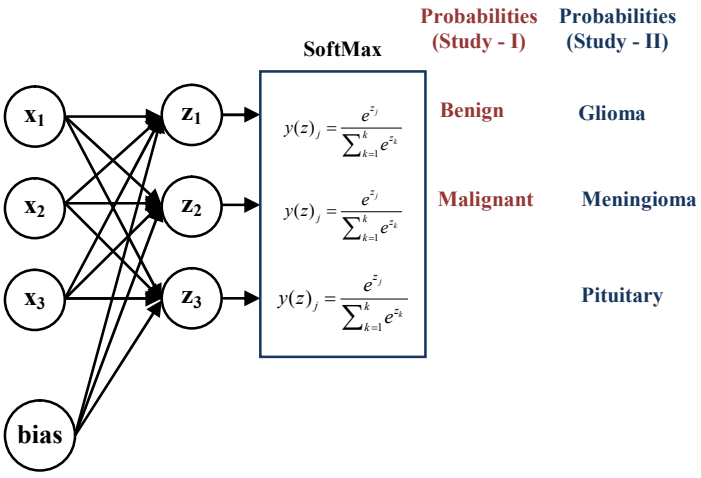

Figure 10: Softmax layer

Based on the loss of cross-entropy to estimate the loss of classification and provides the final categorical label for each image input by the classification layer. Loss can be calculated from the following equation, where p is the vector of the target labels, and q (x) is the softmax layer output vector.

$$H(p,q) = -\sum_{x} ((p(x) * \log((q(x))) \tag{4}$$

3. Validation Metrics

The following are the Validation metrics considered to evaluate the proposed T-Net model. The following are the performance metrics based on TP, FP, TN and FN.

$$\text{Accuracy} = \frac{T_P + T_N}{T_P + T_N + F_P + F_N} \tag{5}$$

$$\text{Sensitivity} = \frac{T_P}{T_P + F_N} \tag{6}$$

$$\text{Specificity} = \frac{T_N}{T_N + F_P} \tag{7}$$

$$\text{Precision} = \frac{T_P}{T_P + F_P} \tag{8}$$

$$\text{F1-Score} = 2\frac{PPV * TPR}{PPV + TPR} \tag{9}$$

4. EXPERIMENTAL RESULTS AND DISCUSSIONS

4.1 Results of Study-I

Figure 11 shows, training accuracy, validation and training loss graph for Study-I. The training accuracy almost 99% after 10000 iterations and loss is less than 0.3. At the end of the training, the overall accuracy reached 97%. The accuracy curve in increases exponentially and there is several variations because of the use of a limited 32-batch sample images. Figure 12 shows the confusion matrix and table 4 shows the validation metrics of study-I.

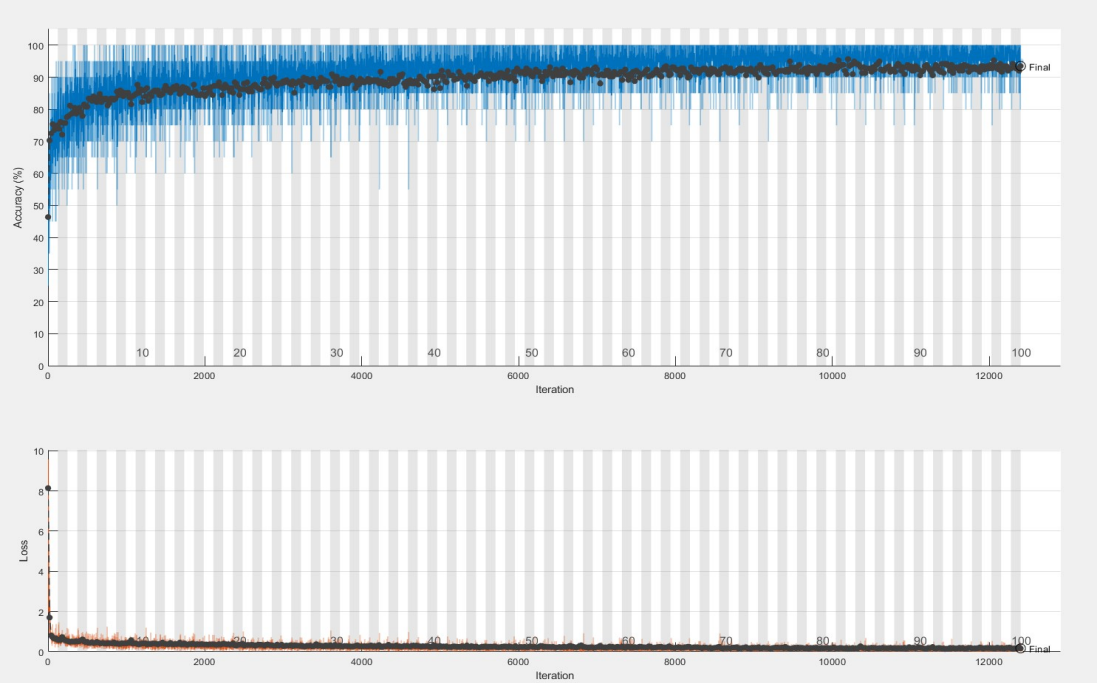

Figure 11: Training accuracy and loss graph for Study-I

The T-Net model achieved 97.96% of for BTDS-3 dataset. The Accuracy comparison plot of previous State of the art methods with proposed T-Net model is shown in figure 13.

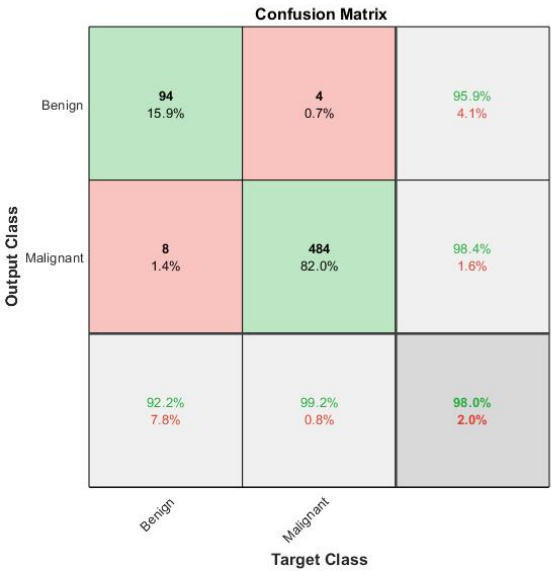

Figure 12: Confusion Matrix for BTDS-3 Data (Study-I)

Table 4: Validation metrics of T-Net for BTDS-3 Data (Study-I)

T-Net Model (Study-I)	
Parameter	**Value**
TP	484
TN	94
FP	8
FN	4
Accuracy	97.96%
Sensitivity	99.18%
Specificity	92.15%
Precision	98.37%
F1-Score	98.77%

4.2 Results of Study-II

Figure 14 shows, training accuracy, validation and training loss graph for Study-II. The training accuracy almost 100% after 10000 iterations and the loss is less than 0.2. At the end of the training, the overall accuracy reached 99.3%. The accuracy curve in increases exponentially and there is Several variations because of the use of a limited 32-batch sample. Figure 15 shows the confusion matrix and table 5 shows the validation metrics of study-II.

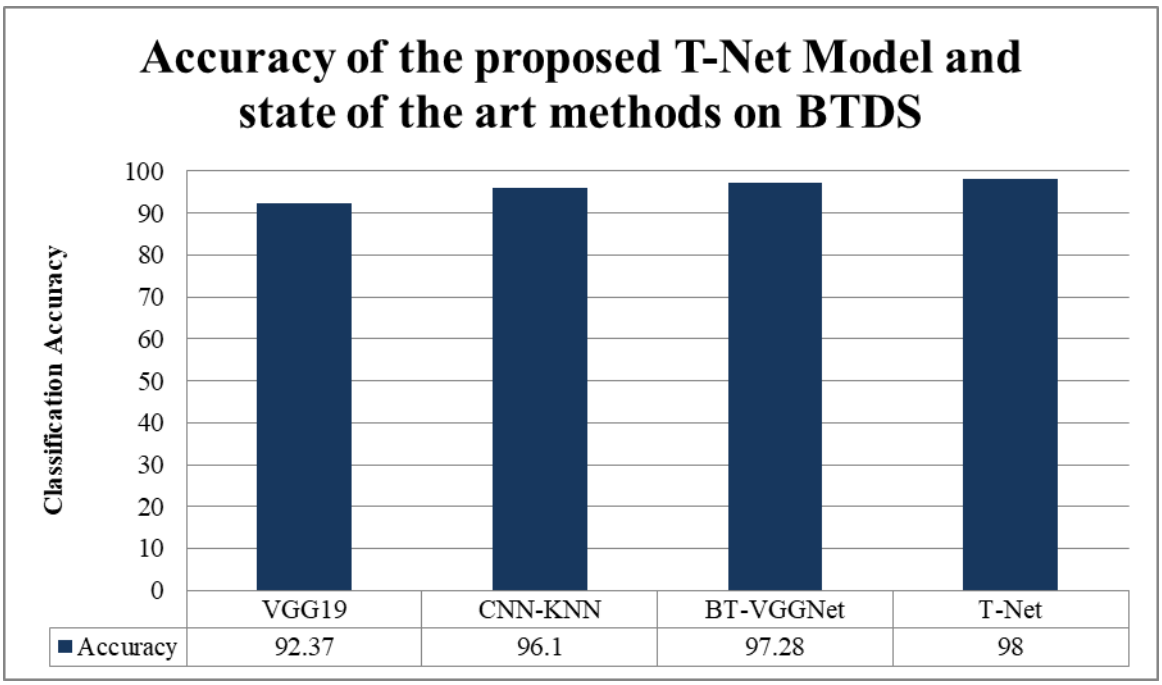

Figure 13: Accuracy comparison with state of art methods plot on BTDS-3 Data (Study-I)

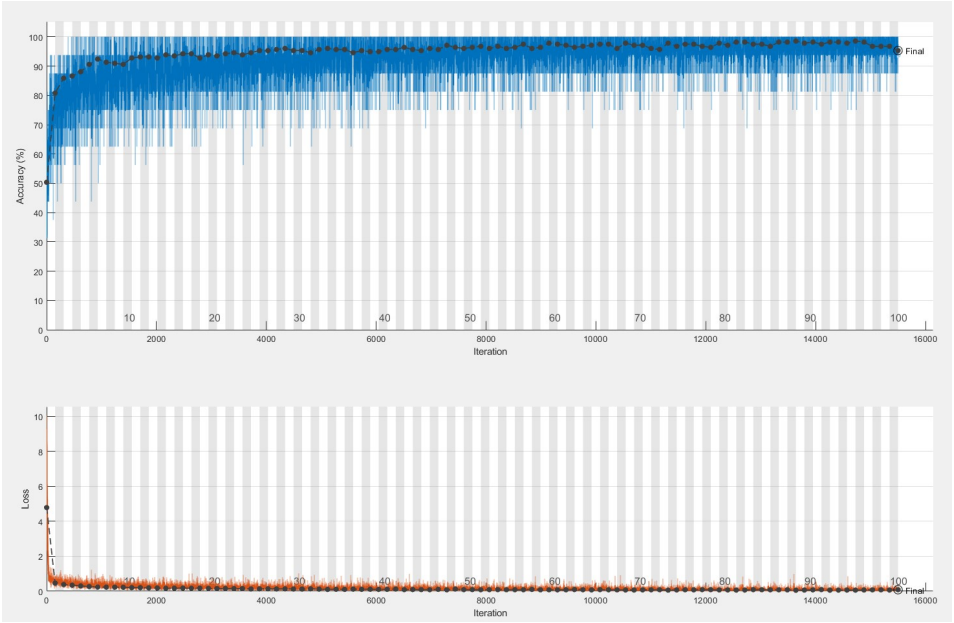

Figure 14: Training accuracy and loss graph for Study-II

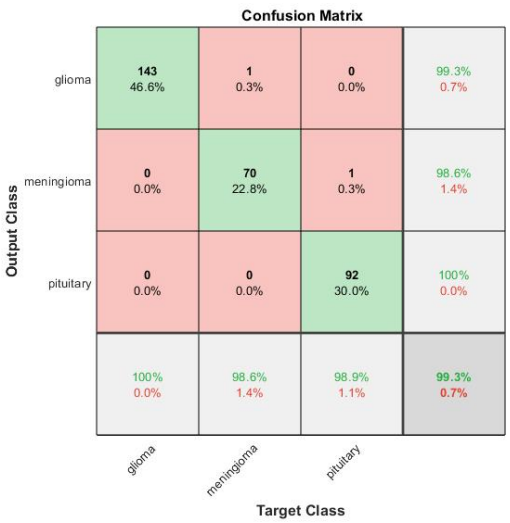

Figure 15: Confusion Matrix for CE-MRI Data (Study-II)

The T-Net model achieved 99.34% of for CE-MRI dataset. The Accuracy comparison plot of previous State of the art methods with proposed T-Net model is shown in figure 16.

Table 5: Validation metrics of T-Net for CE-MRI Data (Study-II)

T-Net Model (Study-II)	
Parameter	**Value**
Accuracy	99.34%
Sensitivity	99.17%
Specificity	99.29%
Precision	98.71%
F1-Score	98.94%

Table 6: Validation metrics of T-Net for individual classes of CE-MRI Data (Study-II)

S.NO	Deep learning Model	Type of Tumor	Sensitivity	Specificity	Precision	F1-Score
1.	T-Net	Glioma	100	98.78	98.62	99.30
		Meningioma	98.59	99.57	98.59	98.59
		Pituitary	98.92	99.53	98.92	98.92

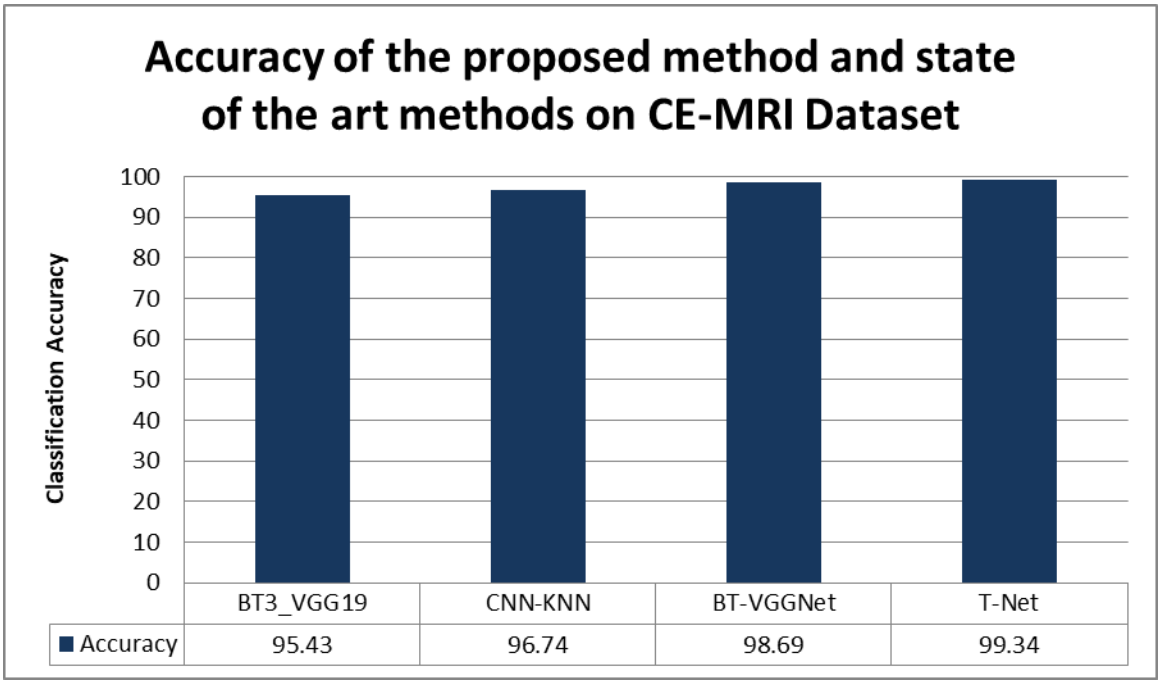

Figure 16: Accuracy comparison with previous methods plot on CE-MRI Data (Study-II)

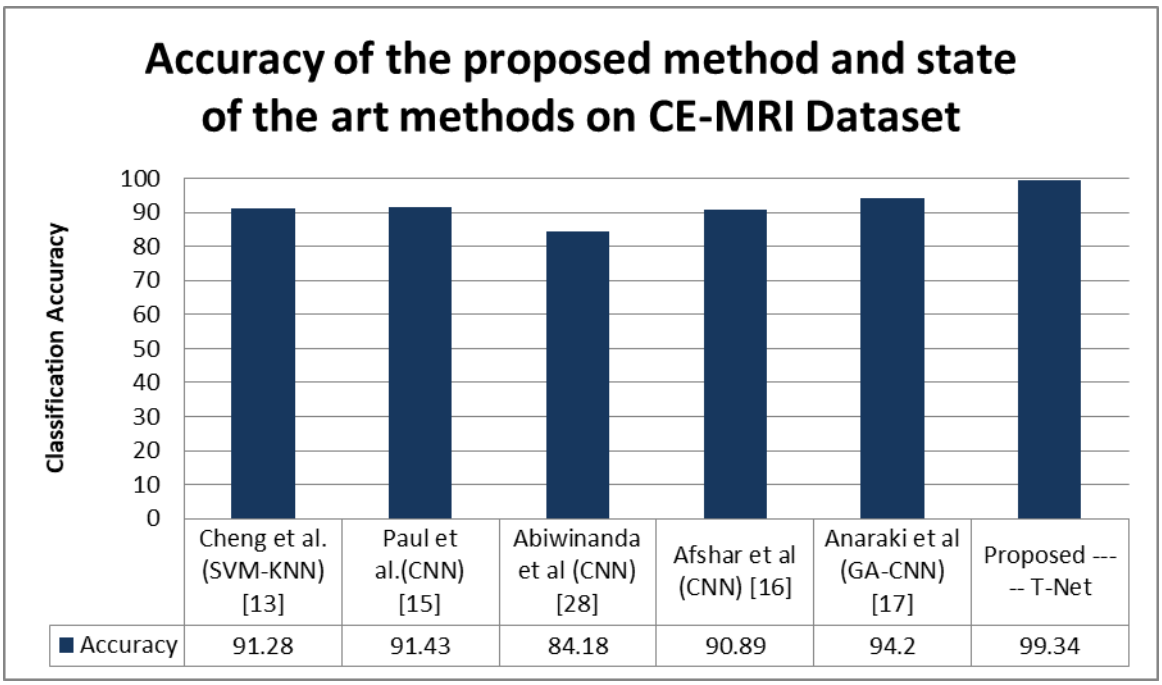

Figure 17: Accuracy comparison with state of art methods plot on CE-MRI Data (Study-II)

5. CONCLUSION

A CAD method for classifying brain tumor MR images into two types (Benign and Malignant) in one study and further classifying multi-tumor into various types (Gliomas, Meningioma, pituitary) using a deep neural network is proposed in this research. The proposed deep neural network (T-Net) is built using 16 layers consists different layers like image input layer to process the images feeding through the convolution layers and their activation functions. Moreover, one dropout layer is adopted to avoid over fitting and followed by a three fully connected layer. For probability distribution and classification, a softmax layer and classification layer utilized to produce the predicted class label. The 2D dataset is taken from BRATS volumetric data. The proposed deep learning architecture has outperformed compared to state of the art models with highest accuracy of 98% and 99.3% concerning the BTDS-3 and CE-MRI datasets respectively.

REFERENCES

1. L. M. De Angelis, "**Brain tumors**," New England J. Med., vol. 344, no. 2, pp. 114_123, Jan. 2001. https://doi.org/10.1056/NEJM200101113440207
2. A. Behin, K. Hoang-Xuan, A. F. Carpentier, and J.-Y. Delattre, "**Primary brain tumours in adults**," Lancet, vol. 361, no. 9354, pp. 323-331, 2003.
3. B. W. Stewart and C. P. Wild, **World Cancer Report 2014**. Lyon, France: IARC, 2014.
4. G. Litjens, T. Kooi, B. E. Bejnordi, A. A. A. Setio, F. Ciompi, M. Ghafoorian, J. A. W. M. van der Laak, B. van Ginneken, and C. I. Sánchez, "**A survey on deep learning in medical image analysis,**" Med. Image Anal., vol. 42, pp. 6088, Dec. 2017. https://doi.org/10.1016/j.media.2017.07.005
5. C. Tas et al., "**Discriminating schizophrenia and schizo-obsessive disorder: A structural MRI study combining VBM and machine learning methods,**"Neural Comput. Appl., vol. 29, no. 2, pp. 377-387, 2018. https://doi.org/10.1007/s00521-016-2451-0
6. D. G. Lowe, "**Distinctive image features from scale-invariant keypoints**," Int. J. Comput. Vis., vol. 60, no. 2, pp. 91110, 2004.
7. A. Ben-Hur, C. S. Ong, S. Sonnenburg, B. Scholkopf, and G. Ratsch, "**Support vector machines and kernels for computational biology,**" PLOS Comput. Biol., vol. 4, no. 10, pp. 1-10, 2008. https://doi.org/10.1371/journal.pcbi.1000173
8. L.Wang, H. Shen, F. Tang, Y. Zang, and D. Hu, "**Combined structural and resting-state functional MRI analysis of sexual dimorphism in the young adult human brain: An MVPA approach**," NeuroImage, vol. 61, no. 4, pp. 931-940, 2012.
9. G. Litjens et al., "**A survey on deep learning in medical image analysis**," Med. Image Anal., vol. 42, pp. 60-88, Dec. 2017. https://doi.org/10.1016/j.media.2017.07.005

10. O. Russakovsky et al., "**ImageNet large scale visual recognition chal-lenge**," Int. J. Comput. Vis., vol. 115, no. 3, pp. 211-252, Dec. 2015.
11. E. I. Zacharaki, S. Wang, S. Chawla, D. S. Yoo, R. Wolf, E. R. Melhem, and C. Davatzikos, "**Classication of brain tumor type and grade using MRI texture and shape in a machine learning scheme**," Magn. Reson. Med., vol. 62, no. 6, pp. 1609-1618, Dec. 2009. https://doi.org/10.1002/mrm.22147
12. E. S. A. El-Dahshan, T. Hosny, and A. B. M. Salem, "**Hybrid intelligent techniques for MRI brain images classication**," Digit. Signal Process., vol. 20, pp. 433-441, Mar. 2010. https://doi.org/10.1016/j.dsp.2009.07.002
13. J. Cheng, W. Huang, S. Cao, R. Yang, W. Yang, Z. Yun, Z. Wang, and Q. Feng, "**Enhanced performance of brain tumor classication via tumor region augmentation and partition**," PloS ONE, vol. 10, no. 10, Oct. 2015, Art. no. e0140381.
14. M. G. Ertosun and D. L. Rubin, "**Automated grading of gliomas using deep learning in digital pathology images: A modular approach with ensemble of convolutional neural networks,**" in Proc. AMIA Annu. Symp. Proc., vol. 2015, Nov. 2015, pp. 1899-1908.
15. J. S. Paul, A. J. Plassard, B. A. Landman, and D. Fabbri, "**Deep learning for brain tumor classication**," Proc. SPIE, Med. Imag., Biomed. Appl. Mol., Struct., Funct. Imag., vol. 10137, Mar. 2017, Art. no. 1013710. doi: 10.1117/12.2254195.
16. P. Afshar, K. N. Plataniotis, and A. Mohammadi, "**Capsule networks for brain tumor classication based on MRI images and course tumor boundaries**," 2018, arXiv:1811.00597. [Online]. Available: https://arxiv.org/abs/1811.00597
17. A. K. Anaraki, M. Ayati, and F. Kazemi, "**Magnetic resonance imagingbased brain tumor grades classication and grading via convolutional neural networks and genetic algorithms,**" Biocybernetics Biomed. Eng., vol. 39, no. 1, pp. 63-74, Jan./Mar. 2019. https://doi.org/10.1016/j.bbe.2018.10.004
18. Menze BH, Jakab A, Bauer S, Kalpathy-Cramer J, et. al. "**The Multimodal Brain Tumor Image Segmentation Benchmark (BRATS)**", IEEE Transactions on Medical Imaging 34(10), 1993-2024 (2015) DOI: 10.1109/TMI.2014.2377694
19. Bakas S, Akbari H, Sotiras A, Bilello M, Rozycki M, Kirby JS, Freymann JB, Farahani K, Davatzikos C. "**Advancing The Cancer Genome Atlas glioma MRI collections with expert segmentation labels and radiomic features**", Nature Scientific Data, 4:170117 (2017) DOI: 10.1038/sdata.2017.117
20. Yushkevich, Paul A., and Guido Gerig. "**ITK-SNAP: an intractive medical image segmentation tool to meet the need for expert-guided segmentation of complex medical images**." IEEE pulse 8.4 (2017): 54-57.
21. A. Krizhevsky, I. Sutskever, and G. E. Hinton, "**ImageNet classification with deep convolutional neural networks**," in Proc. Adv. Neural Inf. Process. Syst. (NIPS), Jan. 2012, pp. 1097-1105.
22. Y. LeCun, L. Bottou, Y. Bengio, and P. Haffner, ``**Gradient-based learning applied to document recognition**," Proc. IEEE, vol. 86, no. 11, pp. 2278_2324, Nov. 1998. https://doi.org/10.1109/5.726791
23. S. Ioffe and C. Szegedy, "**Batch normalization: Accelerating deep network training by reducing internal covariate shift**," 2015, arXiv:1502.03167. [Online]. Available: https://arxiv.org/abs/1502.03167
24. V. Nair and G. E. Hinton, "**Rectied linear units improve restricted boltzmann machines**," in Proc. 27th Int. Conf. Mach. Learn. (ICML), 2010, pp. 807-814.
25. J. Nagi, F. Ducatelle, G. A. D. Caro, D. Ciresan, U. Meier, A. Giusti, F. Nagi, J. Schmidhuber, and L. M. Gambardella, "**Max-pooling convolutional neural networks for vision-based hand gesture recognition**," in Proc. IEEE Int. Conf. Signal Image Process. Appl. (ICSIPA), Nov. 2011, pp. 342-347. https://doi.org/10.1109/ICSIPA.2011.6144164
26. N. Srivastava, G. Hinton, A. Krizhevsky, I. Sutskever, and R. Salakhutdinov, "**Dropout: A simple way to prevent neural networks from overtting**," J. Mach. Learn. Res., vol. 15, no. 1, pp. 1929-1958, 2014.
27. N. M. Nasrabadi, "**Pattern recognition and machine learning**," J. Electron. Imag., vol. 16, no. 4, 2007, Art. no. 049901. https://doi.org/10.1117/1.2819119
28. Abiwinanda, N., Hanif, M., Hesaputra, S. T., Handayani, A., & Mengko, T. R. (2019). **Brain tumor classification using convolutional neural network.** In World Congress on Medical Physics and Biomedical Engineering 2018 (pp. 183-189). Springer, Singapore https://doi.org/10.1007/978-981-10-9035-6_33